Gradient band gap engineered alloyed quaternary/ternary CdZnSeS/ZnSeS quantum dots: an ultrasensitive fluorescence reporter in a conjugated molecular beacon system for the biosensing of influenza virus RNA

Gradient Band Gap Engineered Alloyed Quaternary/Ternary CdZnSeS/ZnSeS Quantum Dots: An Ultrasensitive Fluorescence Reporter in a Conjugated Molecular Beacon System for the Biosensing of Influenza Virus RNA

Oluwasesan Adegoke,[†] Min-Woong Seo,[‡] Tatsuya Kato,[†,§] Shoji Kawahito,[‡] Enoch Y. Park[*,†,§]

[†] Laboratory of Biotechnology, Research Institute of Green Science and Technology, Shizuoka University, 836 Ohya, Suruga-ku, Shizuoka 422-8529, Japan

[‡] Imaging Devices Laboratory, Research Institute of Electronics, Shizuoka University, Johoku 3-5-1,Naka-ku, Hamamatsu 432-8011, Japan

[§] Laboratory of Biotechnology, Department of Bioscience, Graduate School of Science and Technology, Shizuoka University, 836 Ohya, Suruga-ku, Shizuoka 422-8529, Japan

Ⓢ *Supporting information*

E-mail:
adegoke.sesan@mailbox.co.za (OA)
mwseo@idl.rie.shizuoka.ac.jp (MS)
kawahito@idl.rie.shizuoka.ac.jp (SK)
kato.tatsuya@shizuoka.ac.jp (TK)
park.enoch@shizuoka.ac.jp (EYP)

[*] Correspondence: Laboratory of Biotechnology, Department of Applied Biological Chemistry, Faculty of Agriculture, Shizuoka University, 836 Ohya, Suruga-ku, Shizuoka 422-8529, Japan. E-mail: park.enoch@shizuoka.ac.jp

ABSTRACT

Controlling and engineering the particle composition of semiconductor alloy is one of the topmost targets in the field of semiconductor material science and technology. Quantum dot (QD) nanocrystals offer an unmatched opportunity to obtain a wide range of composition-controlled alloys and have captivated a great deal of interest recently. Here we report on the band gap engineering via tuning and control of the sulphur molar fraction (ternary shell layer) of quaternary/ternary core/shell alloyed CdZnSeS/ZnSeS QDs. Varying optical properties were exhibited by the alloyed QDs but a uniform particle size distribution was maintained across all compositions. The alloyed QDs displayed bright emission colours under UV irradiation whilst the photoluminescence quantum yield (PL QY) were in a remarkable range of 36 – 98%. Non-linearity of the lattice parameter was an indication of gradient alloying of the nanocrystals while kinetics of the optical properties unravelled the effect of intrinsic optical bowing. The displacement of bond length and anion mismatch influenced the optical properties of the QDs with respect to the PL QY variation. Alloyed CdZnSeS/$ZnSe_{1.0}S_{1.3}$ QDs with a spectacular PL QY value was exploited as an ultrasensitive fluorescence reporter in a conjugated molecular beacon (MB) assay to detect influenza virus H1N1 RNA. Our detection system was rapid, highly sensitive to detect extremely low concentrations of H1N1 RNA (down to 2 copies/mL), specific and versatile (detects H1N1 RNA in human serum). For proof of concept, the alloyed CdZnSeS/$ZnSe_{1.0}S_{1.3}$ QD-MB bioprobe exhibited a superior 12-fold sensitivity over alloyed CdZnSeS-MB probe while conventional CdSe/ZnS-MB probe could not detect the extremely low concentrations of influenza virus H1N1 RNA.

KEYWORDS: Quantum dots, alloy, influenza virus, RNA, photoluminescence, molecular beacon

1. Introduction

At the nanoscale, a great deal of attention has been ascribed to band gap engineering as a powerful tool in the fabrication of semiconductor quantum dots (QDs) nanocrystals.[1-4] Conventional method of tuning the semiconductor band gap is by altering the QDs size in a process known as quantum confinement. QDs produced by size confinement have found application in a wide array of fields, such as in biological imaging, photovoltaics, catalysis, optoelectronics, sensor/biosensor and drug delivery systems, etc.[5-8] In many applications, QDs of small size are required to obtain distinct data, however, the significant size difference between QDs of different emission colors poses a serious problem in device processing, superlattice structure formation and biomolecule conjugation.[9,10] Hence, tuning the optical properties of QDs independent of their size is highly needed to circumvent this problem.

An alternative means of engineering the band gap of QD nanocrystals is via control and alteration of the particle composition with respect to changes in the stoichiometry of the semiconductor metal molar fraction.[9] This process produces alloyed QDs nanocrystals of different compositions. Several groups have shown that alloyed QDs possess superior output efficiency over conventional QD systems. For example, Krauss et al.[11] demonstrated "nonblinking" properties in alloyed CdZnSe/ZnSe QDs. Solar cell application of alloyed ternary $PbSe_xSe_{1-x}$ QDs was shown by Alivisatos et al.[12] to exhibit 2-fold improvement in efficiency over PbSe and

PbS-based devices. Light emitting diodes using alloyed ternary ZnCdSe QD were demonstrated by Bawendi et al.[13] to induce charge injection easily than conventional CdSe/ZnS QD. This boost in performance of alloyed QDs for different applications may present an alternative route to invent the next generation of QDs.

Here we report for the first time on the fabrication of water-soluble quaternary/ternary alloyed CdZnSeS/ZnSeS QDs of different compositions but with a fixed uniform size distribution. Variation of the particle composition was performed via tuning and control of the sulphur (S) molar fraction source in the ternary alloyed shell layer. Demonstration of the superior qualities of the alloyed CdZnSeS/ZnSeS QDs as an ultrasensitive fluorescence signal generator in a conjugated molecular beacon (MB) assay system was exploited to detect extremely low concentrations of influenza virus H1N1 RNA. For proof of concept, we compared the signal efficiency of our alloyed QD-MB bioprobe with the signal read-out generated from core alloyed CdZnSeS-MB and conventional CdSe/ZnS QD-based MB probe systems. Particularly, monitoring the interaction between a reporter and molecule is a requirement to achieve specific detection in biosensing. The alloyed QD-MB bioprobe with a DNA oligonucleotide sequence was designed to hybridize with H1N1 viral RNA sequence. The hybridization effect induced the alloyed QD reporter in the conjugated MB system to transduce molecular recognition information for H1N1 viral RNA into unparalleled optical signals.

Acute infectious respiratory disease known as influenza virus are single stranded RNA viruses belonging to the family of *Orthomyxoviridae*. Infection caused by influenza virus occurs with varying attack rates and severity depending on the strain

of the virus subtype that is involved.[14,15] Techniques used to diagnose influenza virus have come with several criticism. For example, when using the nasopharyngeal aspirates and swabs technique, samples with low viral copies degrades the RNA, hence limiting the quantification by polymerase chain reaction (PCR).[16] Serological diagnosis based on antibody detection generates data that are not interpretable and often misguided.[17] Viral culture test are time consuming[18] while the commercial rapid influenza detection test (RIDTS) is known to consistently generate false positive or false negative results.[19] Lastly, fluorescence antibody assays are cheap and offer fast results but they exhibit low sensitivity.[20] Hence, influenza virus-based probes that can generate accurate data in combination with high sensitivity and rapidity are urgently needed to enable swift point-of-care treatment and disease control.

The nanodiagnostic bioprobe developed in this work is rapid, specific and ultrasensitive to detect influenza virus H1N1 RNA down to 2 copies/mL. The versatility of our probe system was demonstrated for the detection of the target viral RNA in complex biological matrix using human serum as a detection medium. Our report is the first to exploit an ultrasensitive alloyed quaternary/ternary QD-MB bioprobe for the biosensing of influenza virus H1N1 RNA.

2. Experimental section

2.1. Materials

Cadmium oxide (CdO), octadecene (ODE), zinc oxide (ZnO), trioctylphosphine oxide (TOPO), trioctylphosphine (TOP), selenium (Se), hexadecylamine (HDA), sulphur, thioglycolic acid (TGA), rhodamine 6G, N-(3-dimethylaminopropyl)-N'-

ethylcarbodiimide hydrochloride (EDC) and N-hydroxysuccinimide (NHS) were purchased from Sigma Aldrich Co. LLC. (Saint Louis, MO, USA). Oleic acid (OA) was purchased from Nacalai Tesque Inc. (Kyoto, Japan). Potassium hydroxide (KOH), methanol, acetone, and chloroform were purchased from Wako Pure Chemical Ind. Ltd. (Osaka, Japan). An ultra-pure Milli-Q Water System was used as the water source. Purified dengue 1 virus RNA and influenza virus A/California/07/2009 (H1N1) were purchased from Vircell Microbiologists (Granada, Spain). The MB probe has 22 necleotide base pairs that are complimentary to the nucleotide 619–643 neuraminidase (NA) gene of influenza virus A/California/07/2009 (H1N1). H1N1 viral RNA had a stock concentration of 1.45×10^7 copies/mL once reconstituted with 50 µl of RNase free water, hence serial dilution were performed from the stock solution. MB with DNA oligonucleotide was synthesized and purified (using HPLC) by Integrated DNA Technologies (Coralville, IA, USA). The MB consists of 35 bases single-stranded DNA labeled with 5′ amino (NH_2) modifier C6 and 3′ Dabcyl (4-((4-(dimethylamino)phenyl)azo)benzoic acid) fluorescence quencher. The resulting oligonucleotide sequence of the MB is as follow:

5′-/5AmMC6/**GCGAC**TTTCAGTTATTATGCCGTTGTATTT**GTCGC**/Dabcyl/-3′.

The stem domain of the MB probe was created using the underlined bases.

2.2. Synthesis of alloyed CdZnSeS/ZnSeS QDs

Organometallic hot-injection one-pot synthesis of CdZnSeS/ZnSeS QDs was carried out using reported procedures for the fabrication of alloyed QDs[7,21] but with modification. Briefly, 1.3 g of CdO, 0.6 g of HDA, 50 mL ODE and 30 mL OA were

loaded into a 3-necked flask, stirred and heated to ~280 ^{o}C under inert atmosphere. As the temperature of the solution approached ~260 ^{o}C, 2.23 mL of TOP was injected into the Cd-HDA-OA solution. A premixed TOPSe solution (~12 mL), containing 0.3 g of Se and 1.93 g of TOPO in 25 mL of ODE was added into the Cd-OA-HDA complex solution to initiate the nucleation and growth of the binary CdSe seeds. A solution of ZnO (~20 mL), containing 0.407 g of ZnO in 20 mL of OA and 30 mL of ODE was added into the CdSe growth solution, followed swiftly by the addition of TOPS solution (~50 mL) containing 0.16 g of sulphur and 1.93 g of TOPO in 20 mL of OA and 30 mL of ODE to initiate the nucleation and growth of the quaternary alloyed CdZnSeS QDs. The reaction was allowed to proceed for several minutes for effective nucleation and growth of the alloyed quaternary core QDs. Once satisfactory growth of the alloyed core QDs was achieved, a fraction of the solution was injected out and a solution of ZnO, TOPSe and TOPS precursors were added swiftly for the overcoating of the ternary alloyed ZnSeS shell layer. The stoichiometric particle composition of S in the ternary alloyed ZnSeS shell was varied to obtain different alloyed core/shell compositions. The hydrophobic QDs were purified using methanol and acetone.

2.3. Water solubilization of the alloyed QDs

A ligand exchange reaction was carried out using a KOH-methanolic-TGA solution to obtain water-soluble nanocrystals**.** Briefly, 3 g of KOH was dissolved in 40 mL of methanol via ultrasonication and 2 mL of TGA was added and the solution was stirred. Separate solution of the hydrophobic QDs were added into the KOH-methanolic-TGA

solution, followed by the addition of Milli-Q water. The solutions were stirred for several minute and left to stand still overnight for effective separation of the organic phase from the water-soluble phase. The QDs were washed using acetone and chloroform by centrifugation. The purified water-soluble QDs were dried in a fume hood and obtained with high yield.

2.4. Characterization

UV/vis absorption and fluorescence emission measurements were carried out using a filter-based multimode microplate reader (Infinite® F500, TECAN, Ltd, Männedorf, Switzerland). Transmission electron microscopy (TEM) images were performed using TEM JEM-2100F, (JEOL, Ltd., Tokyo, Japan) operated at 100 kV. Powder X-ray diffraction (PXRD) measurements were carried out using a RINT ULTIMA XRD (Rigaku Co., Tokyo, Japan) with a Ni filter and a Cu-Kα source. Data were collected from 2 theta = 5 - 60^{o} at a scan rate of 0.01^{o}/step and 10s/point. FT-IR analysis were carried out using a FT-IR (ATR 8700, Shimadzu Co., Tokyo, Japan). Fluorescence lifetime measurements were performed using a fluorescence lifetime imaging microscopy (FLIM) equipped with a time-resolved CMOS image sensor.[22] Excitation source was a 472 nm laser diode with pulse width of 120 ps and peak power of 48 mW. The cycle period of trigger signal is 192 ns, width of time window is 32 ns, delay step for scanning is 500 ps and sensors intrinsic response at 472 nm laser is 220 ps.

2.5. Preparation of the alloyed QD-MB conjugate

Aqueous solution of the alloyed QDs (2 mL) were mixed with 1.0 mL of 0.1 M EDC and stirred for ~30 min to activate the terminal carboxylic groups. Aqueous solution of 10 nM MB (1 mL) was subsequently added and followed swiftly by the addition of 1.0 mL of 0.1 M NHS solution. The solution was stirred overnight under ambient condition. The QD-MB conjugates were purified and concentrated by centrifugation using a 30,000 Microcon molecular weight cut-off Nanosep® centrifugal filter (Pall Co., Drive Port Washington, NY, USA).

2.6. Fluorescence assay

Influenza virus A/California/07/2009 (H1N1) RNA was detected under optimum conditions using alloyed CdZnSeS/$ZnSe_{1.0}S_{1.3}$-MB bioprobe. Working solution of H1N1 viral RNA were prepared in molecular biology grade water that is free from RNase. In a 96-well plate, separate detection solutions were prepared by mixing a constant volume of 10 µl of the QD-MB probe solution with 50 µl of buffer or human serum and 5 µl of H1N1 viral RNA. This process was repeated for the detection of each concentration of H1N1 viral RNA. The probe solutions were stirred for few seconds and the PL emission was measured after 3 min of hybridization time. The excitation wavelength was fixed at 470 nm and the PL emission range was measured between 480 and 800 nm.

2.7. Fluorescence detection principle

The fluorescence detection principle for influenza virus H1N1 RNA using the alloyed QD-MB bioprobe is demonstrated in Scheme 1. Covalent conjugation of the alloyed QDs to the MB probe triggered the fluorescence quenching of the former due to

Förster resonance energy transfer (FRET). The close proximity between the alloyed QDs and quencher molecule induces energy transfer processes. Hybridization between the loop sequence of the QD-MB bioprobe and the target H1N1 viral RNA nucleotide sequence results in the formation a DNA/RNA heteroduplex which then stretches the distance between the alloyed QD reporter and quencher molecule. Hence, a PL read-out signal is generated in proportion to the concentration of the target RNA.

3. Results and discussion

3.1. Structural properties

PXRD pattern of the QDs shows a characteristic zinc-blend crystal structure for the binary CdSe core, alloyed quaternary CdZnSeS core and all composition of the alloyed quaternary/ternary CdZnSeS/ZnSeS core/shell QDs (Figure 1). The consistent zinc-blend crystalline structure signifies the lack of phase change in the diffraction pattern of the QDs. We have included the diffraction pattern of binary CdSe in order to confirm structural changes in the alloyed QDs. The diffraction peaks are indexed to the scattering planes of {111}, {220} and {311} respectively. Broadening of the diffraction peak width is due to the nano-sized dimension of the nanocrystals. With respect to the 2θ position of the diffraction peaks, the peaks of alloyed CdZnSeS QDs are shifted to higher Bragg angle in comparison to the binary CdSe seed. This confirms structural changes in the alloyed core. Subsequently, the diffraction peaks for alloyed CdZnSeS/ZnSeS QDs are also slightly shifted to higher Bragg angle in comparison to the alloyed CdZnSeS core. Increase in the S composition of the alloyed core/shell

induced no significant peak shift which we assume to be due to gradient alloying of the nanocrystals.

A non-linear relationship between the S composition and the lattice parameter measured from the XRD pattern of alloyed CdZnSeS/ZnSeS QDs was observed (Figure 2). This observation is inconsistent with Vegard's law which interprets a linear relationship as a homogeneous alloy.[23] Due to the non-linearity observed, a gradient alloying structure as well as the creation of residual strain is inherent in the alloyed core/shell QDs. It is reasonable to assume that the non-linear relationship complements the absence of peak shift in the diffraction pattern of the composition-dependent alloyed CdZnSeS/ZnSeS QDs. Studies on the band gap engineering of alloyed CdSeTe QDs have shown a strong nonlinear relationship which was described as "optical bowing".[9] We believe quantum confinement and size confinement are not the factors responsible for the nonlinear effect but rather the composition dependent nature of the alloyed QDs. Reports have shown similarities in the alloying mechanism present in nanoscopic and macroscopic alloys. Based on the model theory proposed by Zunger et al.,[24,25] the nonlinear effect is attributed to three electronic and structural factors: (a) the structure of the compound has different lattice constants, (b) the atomic sizes of the different metal ions are different, and (c) the electronegativity values of the metal ions are different. It is reasonable to assume that at equilibrium positions, band gap reduction and structural ordering in the alloyed CdZnSeS/ZnSeS nanocrystals occur due to the relaxation of the cation-anion bonds. This theory is usually used in predicting the nonlinear composition nature of bulk materials and

hence can be employed as a theoretical model to predict the structural nature of the alloyed core/shell QDs.

TEM images of the alloyed CdZnSeS core and the composition-dependent alloyed CdZnSeS/ZnSeS core/shell QDs are shown in Fig. 3A – G. The particle size distribution of the alloyed QDs were estimated using ImageJ software (http://imagej.nih.gov/ij/, U.S. National Institutes of Health [NIH], Bethesda, Maryland, USA). The estimated particle size distribution of alloyed CdZnSeS is 9 nm while the particle size for the alloyed CdZnSeS/ZnSeS QDs is 10 nm for all compositions. Irrespective of the variation in the S composition, we achieved a uniform particle size distribution across the entire composition of the alloyed core/shell QDs. This phenomenon is one of the stand-out features of alloyed QDs. The shape of the alloyed nanocrystals was consistently spherical across the entire TEM monographs while the particle size distribution was monodispersed. This provides direct evidence of homogenous nucleation of the alloyed nanocrystals. It is important to emphasis that homogenous nucleation represents a mirror image of the particle size distribution of the QDs and does not imply the formation of a homogenous alloy structure. From the analysis of the lattice parameters (described above), the gradient alloying of the QDs was inherent.

The zeta potential curves for the alloyed QDs are presented in Figure S-1 (supporting information). The zeta potentials of the alloyed QDs are negative charged but with striking differences. Alloyed CdZnSeS is more negatively charged than the composition-dependent alloyed CdZnSeS/ZnSeS QDs. It is important to emphasis that the zeta potentials for each nanocrystal is dependent on their polarity in water

and unique for each nanocrystal. The differences are expected due to the varying number of terminal TGA groups anchored on their surface.

3.2. Composition-dependent optical properties

3.2.1. Band gap alloying

Several studies have demonstrated the tuning of the optical properties of alloyed QDs via particle composition.[9,26-28] In our study, the S chalcogenide molar fraction was tuned and controlled in the alloyed core/shell structure. Photographs of the emission colors of the alloyed core and core/shell QDs taken under ambient and UV light are shown in Figure 3H. Each of the alloyed QDs displayed distinct brightness with different emission color of orange (alloy core), red (alloyed core/shell) and reddish-orange (alloyed core/shell) under UV light. This demonstrate that our synthesized alloyed QDs are bright and will serve as effective light-emitting fluorophores for a wide array of biological and chemical applications.

Typical PL emission and absorption spectra of the binary CdSe core, alloyed CdZnSeS core and all composition of the alloyed CdZnSeS/ZnSeS core/shell QDs are shown in Figure 4. Binary CdSe core displayed two excitonic absorption peaks which broadened slightly in the absorption spectrum of the alloyed CdZnSeS core. Further broadening of the excitonic peaks were observed in the absorption spectra of the alloyed core/shell CdZnSeS/ZnSeS QDs. Binary CdSe emitted at 572 nm with a relatively broad PL emission spectrum and full width at half maximum (FWHM) of 60 nm. A deep-trap emission was observed in the low energy region of the spectrum. The deep-trap emission is an indication that CdSe QDs suffers from surface defects. Judging from the PL emission spectra of alloyed CdZnSeS core and CdZnSeS/ZnSeS

core/shell QDs, the deep-trap emission was completely eliminated and a band-edge type of PL emission was formed. Hence, direct evidence of effective surface passivation and suppression of non-radiative exciton recombination was achieved in the alloyed nanocrystals.

Critical assessment of the photophysical properties of the alloyed core/shell QDs showed that the PL emission wavelength did not follow a definite trend. This imply that tuning the particle composition of the alloyed core/shell nanocrystals induced optical band gap variation. To gain meaningful understanding of the optical variation, the plot in relationship of the band gap and emission wavelength maximum of the alloyed core/shell QDs as a function of the S composition are presented in Figure 5A. The relationship of the PL emission wavelength maximum and the band gap as a function of the S composition induced optical bowing. The triggering question is to whether the origination of the band gap variation of the alloyed QDs arises from the composition-dependent factor or from their electronic properties? To unravel this mystery, extrinsic and intrinsic optical bowing have been proposed in literature.[29,30] Extrinsic bowing is ascribed to atomic aperiodicity of short range feature while intrinsic bowing is ascribed to the disorder arising in the crystally ordered semiconductor.[29,30] We have ruled out the possibility of extrinsic bowing effect because defect arising from the short-range aperiodicity have a negligible effect on the nanoscale dimension of the alloyed QDs synthesized in this work. Zunger and Jaffe proposed that in the case of a pseudobinary semiconductor alloy of cubic crystalline nature ($A_xB_{1-x}C$), the atomic displacement of anion from their primary position can induce optical bowing due to the confinement of bond length disorder in the unit

cell.[29] This imply that the displacement of bond length and anion mismatch induced a profound effect on the optical properties of the resulting alloyed QDs which led to optical bowing. Hence, the optical bowing effect arises due to the composition-dependent nature of the alloyed nanocrystals.

3.2.2. PL QY and PL exciton lifetime

One of the photophysical parameters used to judge the quality of any fluorophore is the PL QY. The PL QY value for any given QD can provide information on the effectiveness of the fabrication process used to obtain such nanocrystal and also to unravel the nature of its surface with respect to the effects of passivation. From the analysis of the photophysical properties of the nanocrystals, alloyed CdZnSeS QDs produced a remarkable PL QY value of 85% which is ~43 fold higher than the binary CdSe seed (PL QY = 2%). This remarkable PL QY value of alloyed CdZnSeS QDs is an indication of suppressed non-radiative state. To the best of our knowledge, the spectacular QY value obtained for water-soluble alloyed CdZnSeS QDs in this work is higher than the value of 65% reported by Deng et al..[31] In addition, our reported PL QY value is the best for quaternary alloyed CdZnSeS QDs. Quite intriguingly, alloyed CdZnSeS/$ZnSe_{1.0}S_{1.3}$ and CdZnSeS/$ZnSe_{1.0}S_{1.5}$ QDs produced near unity PL QY (than the parent CdZnSeS core) value of 98% and 93%, respectively. This provides direct evidence of further suppression of non-radiative recombination state in the alloyed core/shell nanocrytals. It is quite surprising that the PL QY of CdZnSeS/$ZnSe_{1.0}S_{1.4}$ (QY = 58%), CdZnSeS/$ZnSe_{1.0}S_{1.6}$ (QY = 66%), CdZnSeS/$ZnSe_{1.0}S_{1.7}$ (QY = 36%) and CdZnSeS/$ZnSe_{1.0}S_{1.8}$ (QY = 51%) QDs were lower in comparison to the spectacular QY

value obtained for CdZnSeS/$ZnSe_{1.0}S_{1.3}$ and CdZnSeS/$ZnSe_{1.0}S_{1.5}$ QDs. With the exception of CdZnSeS/$ZnSe_{1.0}S_{1.7}$ QDs, the PL QY of the rest of the alloyed core/shell QDs are greater than 50%, which we believe are high from a scientific point of view. Differences in the PL QY justifies the alloying process of QD nanocrystals in which tuning of the optical properties can be achieved without size alteration. Hence, we have obtained in this work, alloyed quaternary/ternary core/shell QDs of the same size but with different photophysical properties.

Plots of the PL QY and FWHM as a function of the S molar fraction are shown in Figure 5B. An improvement in the FWHM of the alloyed core and core/shell QDs over binary CdSe core was achieved. The FWHM of the alloyed core and core/shell QDs ranged narrowly between 35 and 40 nm. The plot of the PL QY as a function of the S composition, reveals the photophysical changes in the alloyed QDs (shown in Figure 5B graphically). Logically, it is reasonable to affirm that a composition-dependent optical variation is inherent in the alloyed core/shell QDs. It is known that residual strain can reduce the band gap of semiconductor materials and thus lead to deformed potentials.[32] Recently, Kwon and coworkers used empirical pseudopotential modelling to unravel the mystery behind the band gap variation of quaternary alloy $Cd_xZn_{1-x}S_ySe_{1-y}$ QDs of different structural nature namely; nanosheets (NSs), nanobelts (NBs) and nanowires (NWs).[33] Their model data showed that the optical bowing effect in CdZnSeS NSs and NBs was induced by residual strain. A semiemperical model interpreted the residual strain to arise from mismatch bond length due to intrinsic atomic disorder in which the width-to-thickness ratio of the NSs and NBs was a function of the strain relaxation factor.[33] Their model data

complemented the optical bowing effect of the respective nanocrystals. We can unambiguously attribute the variation in the optical properties of the alloyed core/shell QDs to be due to inherent residual strains which varied between each of the nanocrystals. CdZnSeS/$ZnSe_{1.0}S_{1.3}$ and CdZnSeS/$ZnSe_{1.0}S_{1.5}$ with spectacular PL QY were not susceptible to unrelaxed residual strains. However, for the rest of the alloyed core/shell QDs, their PL QY value is a mirror image of the extent of inherent residual strain, i.e, the lower the PL QY, the higher is the residual strain effect.

The PL decay curves for alloyed CdZnSeS core and alloyed CdZnSeS/ZnSeS core/shell QDs are shown in Figure 6A – G. The decay curves for the alloyed nanocrystals are best fitted to monoexponential lifetime values. Each of the alloyed nanocrystals exhibited fast decay lifetimes which were in the range of 2.5 ns to 5.2 ns. The fast exciton lifetimes exhibited by these alloyed nanocrystals is probably due to decrease in the separation of the exciton (electron and hole) wave functions. What is surprising is that there is no direct relationship in the trend of the exciton lifetime with the PL QY values and the amount of S molar fraction in the alloyed nanocrystals. Hence, we conclude that the exciton lifetime properties of the alloyed QDs is dependent on the extent of increase or decrease of their radiative state and overlap of their wave function.[34] Particularly for the alloyed core/shell QDs, the rate of exciton leakage into the shell determined their radiative lifetime value.

3.3. Bioanalytical application of the alloyed QDs

3.3.1. Conjugate confirmation

Alloyed CdZnSeS/$ZnSe_{1.0}S_{1.3}$ QDs with a spectacular PL QY was chosen as an ultrasensitive fluorescence reporter in a conjugated molecular beacon assay to detect influenza virus H1N1 RNA. EDC/NHS coupling chemistry was adopted to conjugate the amino group of the DNA oligo-Dabcyl MB probe with the carboxylic functional group of the alloyed QDs. FT-IR analysis was used as a technique to confirm the formation of the amide bond. As shown in Figure S-2 (supporting information), for the unconjugated alloyed CdZnSeS/$ZnSe_{1.0}S_{1.3}$ QDs, the characteristic band at 1595 cm^{-1} corresponds to the asymmetric –COO functional group while the band at 3373 cm^{-1} corresponds to the broad –OH functional group. Amide bond formation in the QD-MB conjugate is confirmed by the 1^0 amide band at 1566 cm^{-1} and the 2^0 amide band at 1643 cm^{-1}. We emphasis that the band at 3266 cm^{-1} for the QD-MB conjugate can be assigned to the N-H stretching group.

3.3.2. Detection of influenza virus H1N1 RNA

PL emission spectra of the unconjugated alloyed QDs and the QD-MB probe solution (dissolved in buffer and human serum) are shown in Figure 7A. Quenching of the fluorescence of the unconjugated alloyed QDs by the binding effect of the MB probe was apparent. The fluorescence quenching effect fulfills the chemical principle of the binding effect between the MB probe and the QD fluorescence reporter. Detection of influenza virus H1N1 RNA was carried out in buffer and in complex biological matrix using human serum as a detection medium. Fluorescence turn ON detection of extremely low concentrations of H1N1 viral RNA using the QD-MB bioprobe in buffer medium is shown in Figure 7B. It is important to note that the concentration of H1N1

418 viral RNA detected in this work are extraordinary low and detection of such low
419 concentration has not been attempted by any probe to date. From the fluorescence
420 signal spectra, no noticeable peak shift upon detection of H1N1 viral RNA was
421 observed which provides direct evidence of the fluorescence stability of our bioprobe
422 system during the detection period. The corresponding PL calibration curve for the
423 detection of H1N1 viral RNA in buffer is shown in Figure 7C. The limit of detection
424 (LOD) was determined by multiplying the standard deviation of blank measurement
425 (n = 10) by 3 and dividing by the slope of the calibration curve. The calculated LOD
426 obtained is 5.2 copies/mL. Based on the ultimate LOD obtained for the detection of
427 H1N1 viral RNA, it is reasonable to affirm that our alloyed QD-MB bioprobe is
428 ultrasensitive and will be useful as an efficient diagnostic probe for influenza virus
429 H1N1 RNA detection.

430 Versatility of our bioprobe system was exploited for the detection of H1N1 viral
431 RNA in human serum. We have shown in Figure 7D that HINI viral RNA switched
432 on the fluorescence of the alloyed QD-MB probe in a concentration-dependent manner.
433 The corresponding PL signal curve is shown in Figure 7E and the LOD obtained was
434 10.8 copies/mL. The LOD obtained is slightly higher than the value obtained in buffer
435 medium. Nevertheless, we have shown that our bioprobe system is viable to detect
436 H1N1 RNA in complex biological matrix.

437 Table 1 provides a summary of the comparison of the LOD of our system with
438 reported values obtained using molecular test and RIDTS techniques for the detection
439 of influenza virus H1N1 RNA. The comparison shows that our bioprobe system
440 offered improved LOD than the popular molecular test and RIDTS. We believe the

441 superior sensitivity demonstrated by our probe system will make it useful in detecting
442 influenza virus H1N1 in patient during any stage of its infection.
443
444 **3.3.3. Sensitivity comparison and specificity**
445 For proof of concept, we made an attempt to examine the efficacy of TGA-CdZnSeS-
446 MB probe and conventional TGA-CdSe/ZnS-MB probe systems to detect influenza
447 virus H1N1 RNA at the same extremely low concentration detected using the
448 CdZnSeS/$ZnSe_{1.0}S_{1.3}$-MB probe. We found CdZnSeS-MB bioprobe to detect H1N1
449 viral RNA at these low concentrations but very low PL signal was generated. However,
450 conventional CdSe/ZnS could not detect H1N1 viral RNA at these low concentrations.
451 As shown in Figure 8A, the PL intensity signal for the detection of 8 copies/mL of
452 H1N1 viral RNA by CdZnSeS-MB is significantly weaker in comparison to the PL
453 read-out signal generated by CdZnSeS/$ZnSe_{1.0}S_{1.3}$-MB bioprobe. For conventional
454 CdSe/ZnS-MB, the PL signal generated for the detection of 8 copies/mL of H1N1 viral
455 RNA (Figure 8A) was a representation of no detection because the emission intensity
456 was quenched relative to the probe without the target viral RNA. We unambiguously
457 conclude that alloyed CdZnSeS/$ZnSe_{1.0}S_{1.3}$ QDs is a much superior fluorescence signal
458 generator than alloyed CdZnSeS core and far much superior than conventional
459 CdSe/ZnS QDs. The LOD for influenza virus H1N1 RNA using CdZnSeS-MB is 62.8
460 copies/mL. The newly developed CdZnSeS/$ZnSe_{1.0}S_{1.3}$-MB probe is 12-fold more
461 sensitive than CdZnSeS-MB probe.
462 An efficient diagnostic probe must combine not only the qualities of rapid
463 detection and enhanced sensitivity but must be specific to the target analyte. To prove

464 the specificity of the alloyed QD-MB bioprobe for the target influenza virus H1N1
465 RNA, a control experiment using a non-complimentary dengue 1 virus RNA was
466 interacted with the probe and the PL output signal was measured. As shown in Figure
467 8B, the PL signal for 2, 8 and 14 copies/mL of dengue 1 virus RNA detection was weak
468 in comparison to the signal generated for the target influenza virus H1N1 RNA. This
469 confirms that the complimentary H1N1 viral RNA target specifically switched on the
470 fluorescence of our CdZnSeS/$ZnSe_{1.0}S_{1.3}$-MB bioprobe.
471
472 **4. Conclusions**
473 Band gap engineering of alloyed quaternary/ternary CdZnSeS/ZnSeS QDs have been
474 successfully fabricated via control of the S molar fraction for the first time. The optical
475 properties of the alloyed core/shell QDs varied for each composition-dependent
476 nanocrystal but the particle size distribution remained uniform. A spectacular PL QY
477 value of 98% was achieved for the alloyed core/shell nanocrystal. An ultrasensitive
478 alloyed QD-MB bioprobe that can detect extremely low concentrations of influenza
479 virus H1N1 RNA in buffer and in human serum was developed. Our detection system
480 was rapid, ultrasensitive, specific and versatile. We additionally proved that the
481 newly developed CdZnSeS/$ZnSe_{1.0}S_{1.3}$-MB bioprobe was 12-fold more sensitive than
482 CdZnSeS-MB probe while conventional CdSe/ZnS-MB could not detect the low
483 concentrations of the target H1N1 viral RNA. We believe, our detection technique
484 opens the door for further exploitation of viral RNA detection. As we have
485 demonstrated in this work, by careful selection of the RNA nucleotide region, the MB

loop sequence can be designed whilst also taking into consideration the use of a highly sensitive fluorescence reporter to generate unprecedented PL signal.

■ ASSOCIATED CONTENT

Ⓢ Supporting information

Zeta potential curve for the alloyed nanocrystals and FT-IR spectra of the unconjugated alloyed QDs and the QD-MB probe.

■ AUTHORS INFORMATION

Corresponding Author

*E-mail: park.enoch@shizuoka.ac.jp

■ ACKNOWLEDGMENTS

A Japan Society for the Promotion of Science (JSPS) postdoctoral fellowship for overseas researchers (P13454) offered by JSPS is gratefully acknowledged. This work was supported by a Grant-in-Aid for JSPS fellow (No. 26-04354) and in part by the Grant-in-Aid for Scientific Research (S) under Grant 25220905 through the Ministry of Education, Culture, Sports, Science and Technology.

References

(1) K. Boldt, N. Kirkwood, G. A. Beane, P. Mulvaney, *Chem. Mater.,* 2013, **25**, 4731–4738.

(2) M. Dane, K. F. Jensen, C. B. Murray, M. G. Bawendi, *Chem. Matter.,* 1996**, 8**, 173–180.

(3) B. C. Fitzmorris, J. K. Cooper, J. Edberg, S. Gul, J. Guo, J. Z. Zhang, *J. Phys. Chem. C,* 2012, **116**, 25065–25073.

(4) F-C. Liu, T-L. Cheng, C-C. Shen, W-L. Tseng, M-Y. Chiang, *Langmuir,* 2008**, 24**, 2162–2167.

(5) M. J. Ruedas-Rama, E. A. H. Hall, *Anal. Chem.,* 2010**, 82**, 9043–9049.

(6) C-S. Wu, M. K. K. Oo, X. Fan, *ACS Nano,* 2010, **4**, 5897–5904.

(7) Y. Xia, C. Zhu, *Analyst,* 2008**, 133**, 928–932.

(8) C. Yuan, K. Zhang, Z. Zhang, S. Wang, *Anal. Chem.,* 2012**, 84**, 9792–9801.

(9) R. E. Bailey, S. Nie, *J. Am. Chem. Soc.,* 2003, **125**, 7100–7106.

(10) P. O. Anikeeva, J. E. Halpert, M. G. Bawendi, V. Bulovic, *Nano Lett.,* 2009, **9**, 2532–2536.

(11) X. Wang, X. Ren, K. Kahen, M. A. Hahn, M. Rajeswaran, S. Maccagnano- Zacher, J. Silcox, G. E. Cragg, A. L. Efros, T. D. Krauss, *Nature,* 2009, **459**, 686–689.

(12) W. Ma, J. M. Luther, H. Zheng, Y. Wu, A. P. Alivisatos, *Nano Lett.,* 2009, **9**, 2072–2077.

(13) J. M. Caruge, J. E. Halpert, V. Wood, V. Bulovic, M. G. Bawendi, *Nat. Photonics,* 2008, **2**, 247–250.

(14) M. Afilalo, M. Stern, M. Oughton, *Emerg. Med. Clin. North Am.,* 2012, ***30***, 271–305.

(15) E. Crisci, T. Mussá, L. Fraile, M. Montoya, *Mol. Immunol.,* 2013, ***55***, 200–211.

(16) C. L. Ward, M. H. Dempsey, C. J. Ring, R. E. Kempson, L. Zhang, D. Gor, B. W. Snowden, M. Tisdale, *J. Clin. Virol.*, 2004, **29**, 179–188.

(17) Centres for Disease Control and Prevention (CDC). Seasonal Influenza (Flu). Guidance for Clinicians on the Use of Rapid Influenza Diagnostic Tests. Available from URL: http://www.cdc.gov/flu/professionals/diagnosis/clinician_guidance_ridt.htm

(18) J. J. Treanor, Influenza virus. In: G. L. Mandell, J. E. Bennett, R. Dolin, editors. Principles and Practice of Infectious Disease. 2nd ed. Philadelphia, PA: Churchill Livingstone; **2005**. p.2060.

(19) M. L. Landry, *Curr. Opin. Pediatr.,* 2011, **23**, 91–97.

(20) L. Pianciola, G. González, M. Mazzeo, M. Navello, N. Quidel, M. F. Bulgheroni, *Rev. Panam. Salud. Publica.,* 2010, **27**, 452–454.

(21) O. Adegoke, T. Nyokong, P. B. C. Forbes, *J. Alloy Compd.,* 2015**, 645**, 443–449.

(22) M.-W. Seo, K. Kagawa, K. Yasutomi, T. Takasawa, Y. Kawata, N. Teranishi, Z. Li, I. A. Halin, S. Kawahito, *IEEE Int. Solid-State Circuits Conf. (ISSCC) Dig. Tech. Papers*, 2015, 198-199.

(23) L. Vegard, H. Schjelderup, *Phys. Z.,* 1917, **18**, 93.

(24) J. E. Bernard, A. Zunger, *Phys. Rev. B,* 1987, **36**, 3199-3226.

(25) S. H. Wei, S. B. Zhang, A. J. Zunger, *Appl. Phys.,* 2000**, 87**, 1304–1311.

(26) B. C. Fitzmorris, Y-C. Pu, J. K. Cooper, Y-F. Lin, Y-J. Hsu, Y. Li, J. Z. Zhang, ACS *Appl. Mater. Interfaces,* 2013, **5**, 2893-2900.

(27) X. Xia, Z. Liu, G. Du, Y. Li, M. Ma, K. Yao, *J. Lumin.,* 2012, **132**, 100–105.

(28) X. Zhong, Y. Feng, W. Knoll, M. Han, *J. Am. Chem. Soc.,* 2003, **125**, 13559-13563.

(29) A. Zunger, J. E. Jaffe, *Phys. Rev. Lett.,* 1983, **51**, 662–665.

(30) J. A. Van Vechten, T. K. Bergstresser, *Phys. Rev. B,* 1970, **1**, 3351–3358.

(31) Z. Deng, H. Yan, Y. Liu, *J. Am. Chem. Soc.,* 2009, **131**, 17744–17745.

(32) J. Kim, M. V. Fischetti, S. Aboud, *Phys. Rev. B,* 2012, **86**, 205323.

(33) S. J. Kwoon, H. M. Jeong, K. Jung, D-H. Ko, H. Ko, I-K. Han, G. Y. Kim, J-G. Park, *ACS Nano,* 2015**, 9**, 5486–5499.

(34) C. M. Tyrakowski, A .Shamirian, C. E. Rowland, H. Shen, A. Das, R. D. Schaller, P. T. Snee, *Chem. Mater.,* 2015, **27**, 7276–7281.

(35) M. Panning, M. Eickmann, O. Landt, M. Monazahian, S. Ŏlschlăger, S. Baumgarte, U. Reischl, J. J. Wenzel, H. H. Niller, S. Günther, B. Hollmann, D. Huzly, J. F. Drexler, A. Helmer, A. Becker, B. Matz, A. M. Eis-Hübinger, C. Drosten, *Eurosurveillance*, 2009**, 14**, 1–6.

(36) S. B. Munro, J. Kuypers, K. R. Jerome, *J. Clin. Microbiol.,* 2013, **51**, 1124-1129

(37) K-H. Chan, K. K. W. To, J. F. W. Chan, C. P. Y. Li, H. Chen, K-Y.Yuen, *J. Clin. Microbiol.,* 2013, **52**, 3160–3161.

600 **Table 1. Comparison of the LOD of Alloyed CdZnSeS/$ZnSe_{1.0}S_{1.3}$ QD-MB Probe**

601 **with Reported Values for the Detection of Influenza Virus H1N1 RNA**

Probe name	H1N1 Strain	Technique	LOD (copies/mL)	Ref.
CdZnSeS/$ZnSe_{1.0}S_{1.3}$ QD-MB (Dabcyl)	A/California/7/2009	Fluorescence enhancement	5.2	This work
RT-PCR	A (H1N1) 2009	Molecular test	384	35
RT-PCR TaqMan	2009 H1	Molecular test	1000	36
Resplex II Plus	A/HK/415742/09	Molecular test	7.1	37
BD Veritor	A/HK/415742/09	RIDTS	6.1	37
QuickVue	A/HK/415742/09	RIDTS	6.6	37
Influenzatop	A/HK/415742/09	RIDTS	6.9	37

602

Figure legends

Scheme 1. Fluorescence detection principle for the QD-MB nanobioprobe.

Figure 1. Powder XRD pattern of the QDs. A spurious signal is indicated by the asterisk (*).

Figure 2. Calculation from Vegard's law showing the non-linear relationship in the lattice parameter *c* of alloyed CdZnSeS/ZnSeS QDs as a function of the S molar fraction.

Figure 3. TEM images for alloyed (A) CdZnSeS, (B) CdZnSeS/$ZnSe_{1.0}S_{1.3}$, (C) CdZnSeS/$ZnSe_{1.0}S_{1.4}$, (D) CdZnSeS/$ZnSe_{1.0}S_{1.5}$, (E) CdZnSeS/$ZnSe_{1.0}S_{1.6}$, (F) CdZnSeS/$ZnSe_{1.0}S_{1.7}$ and (G) CdZnSeS/$ZnSe_{1.0}S_{1.8}$ QDs. (H) Photograph of the alloyed QDs sample taken under ambient and UV light. From left to right: alloyed CdZnSeS core, CdZnSeS/$ZnSe_{1.0}S_{1.3}$, CdZnSeS/$ZnSe_{1.0}S_{1.4}$, CdZnSeS/$ZnSe_{1.0}S_{1.5}$, CdZnSeS/$ZnSe_{1.0}S_{1.6}$, CdZnSeS/$ZnSe_{1.0}S_{1.7}$ and CdZnSeS/$ZnSe_{1.0}S_{1.8}$ QDs.

Figure 4. UV/vis absorption and PL emission spectra of CdSe, alloyed CdZnSeS and all composition of the alloyed CdZnSeS/ZnSeS QDs.

Figure 5. Plot of the S molar fraction in the alloyed CdZnSeS/ZnSeS nanocrystal as a function of (A) Band gap energy (open circles); PL emission maximum (closed circles) and (B) FWHM (open circles); PL QY (closed circles).

Figure 6. Fluorescence lifetime decay curves for the alloyed QDs.

586 **Figure 7.** (A) PL emission spectra of unconjugated CdZnSeS/$ZnSe_{1.0}S_{1.3}$ before and
587 after conjugation to the MB in buffer and in human serum (B) PL turn ON detection
588 of H1N1 viral RNA in buffer using the TGA-CdZnSeS/$ZnSe_{1.0}S_{1.3}$-MB bioprobe, (C)
589 corresponding PL calibration signal curve for the detection of H1N1 viral RNA in
590 buffer, (D) PL turn ON detection of H1N1 viral RNA in human serum using the TGA-
591 CdZnSeS/$ZnSe_{1.0}S_{1.3}$-MB bioprobe, (C) corresponding PL calibration signal curve for
592 the detection of H1N1 viral human serum. Error bars = standard deviation of three
593 measurements.

594 **Figure 8.** (A) Fluorescence signal intensity of alloyed CdZnSeS/$ZnSe_{1.0}S_{1.3}$ QD-MB
595 probe for the detection of 8 copies/mL of influenza virus H1N1 RNA in comparison
596 to the signal intensity generated by alloyed CdZnSeS-MB probe. (B) Specificity of the
597 alloyed QD-MB probe for H1N1 viral RNA detection using non-complimentary
598 dengue 1 virus RNA as a control. Error bars = standard deviation of three
599 measurements.

Scheme 1, Adegoke et al.

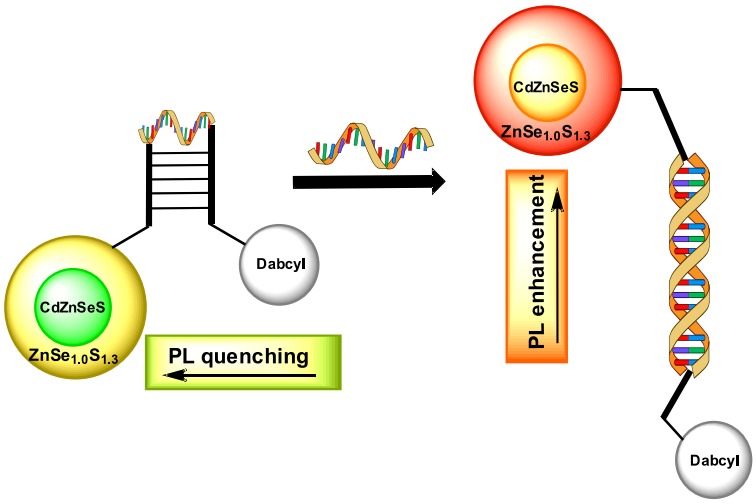

Fig. 1, Adegoke et al.

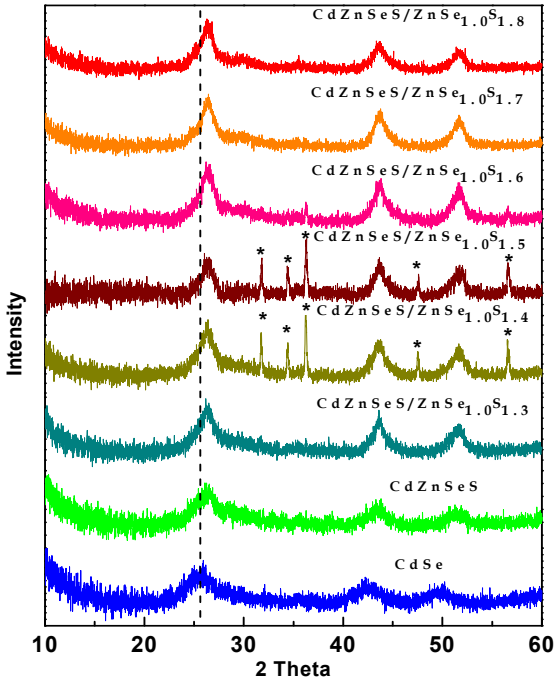

Fig. 2, Adegoke et al.

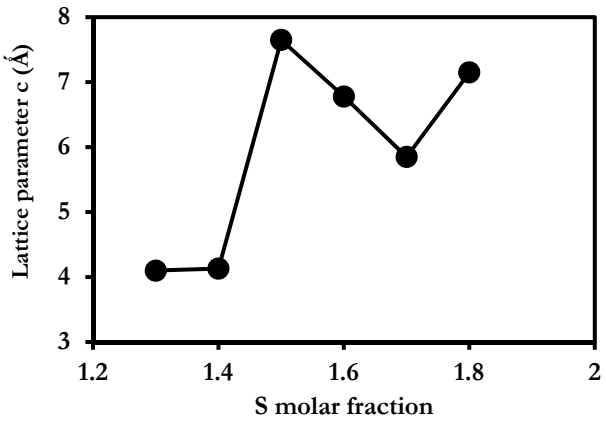

Fig. 3, Adegoke et al.

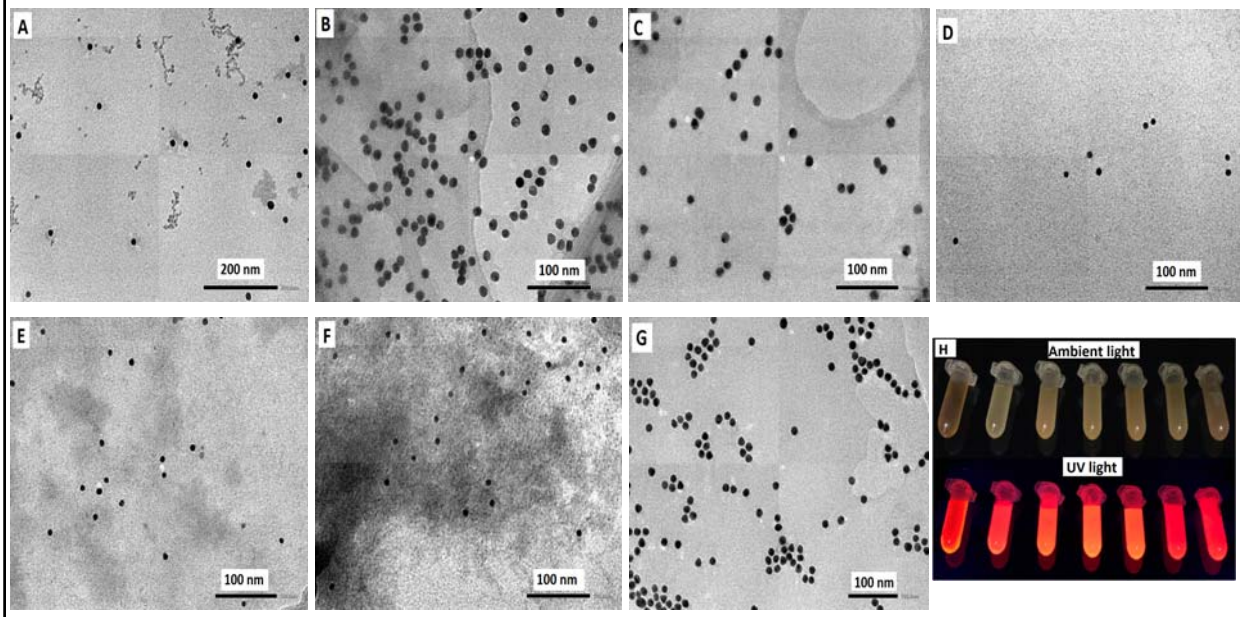

Fig. 4, Adegoke et al.

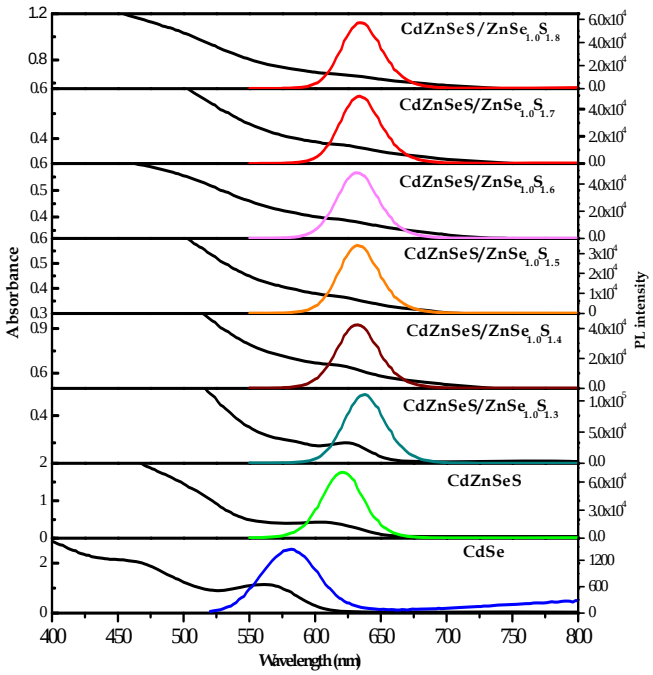

Fig. 5, Adegoke et al.

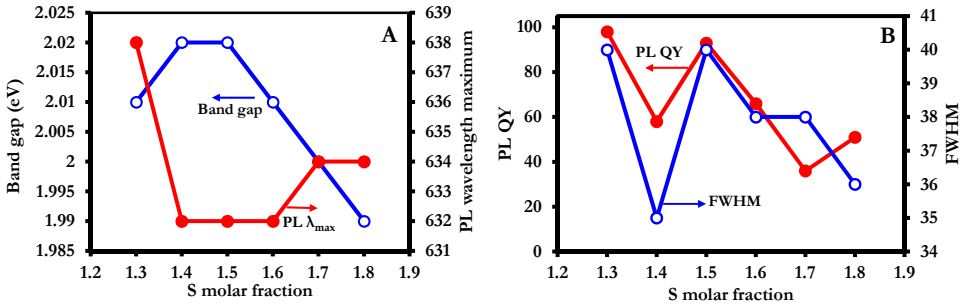

Fig. 6, Adegoke et al.

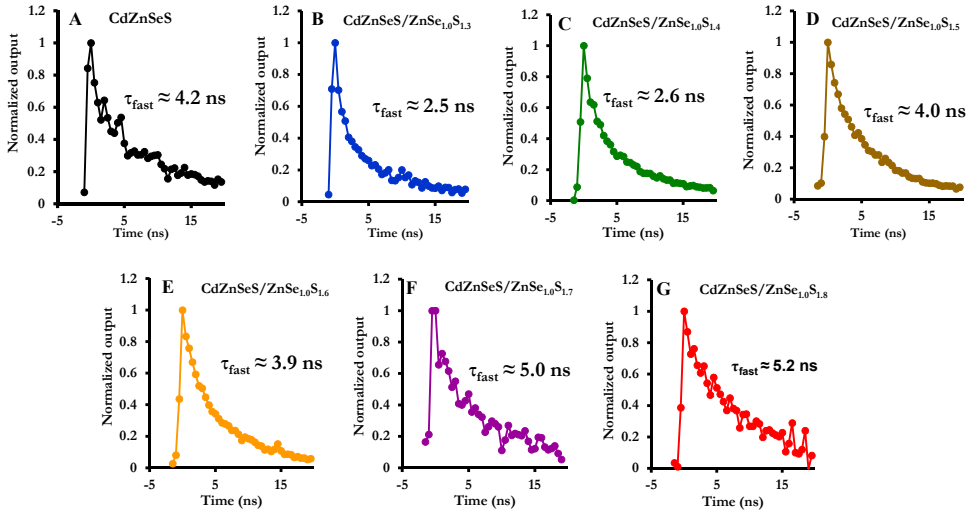

Fig. 7, Adegoke et al.

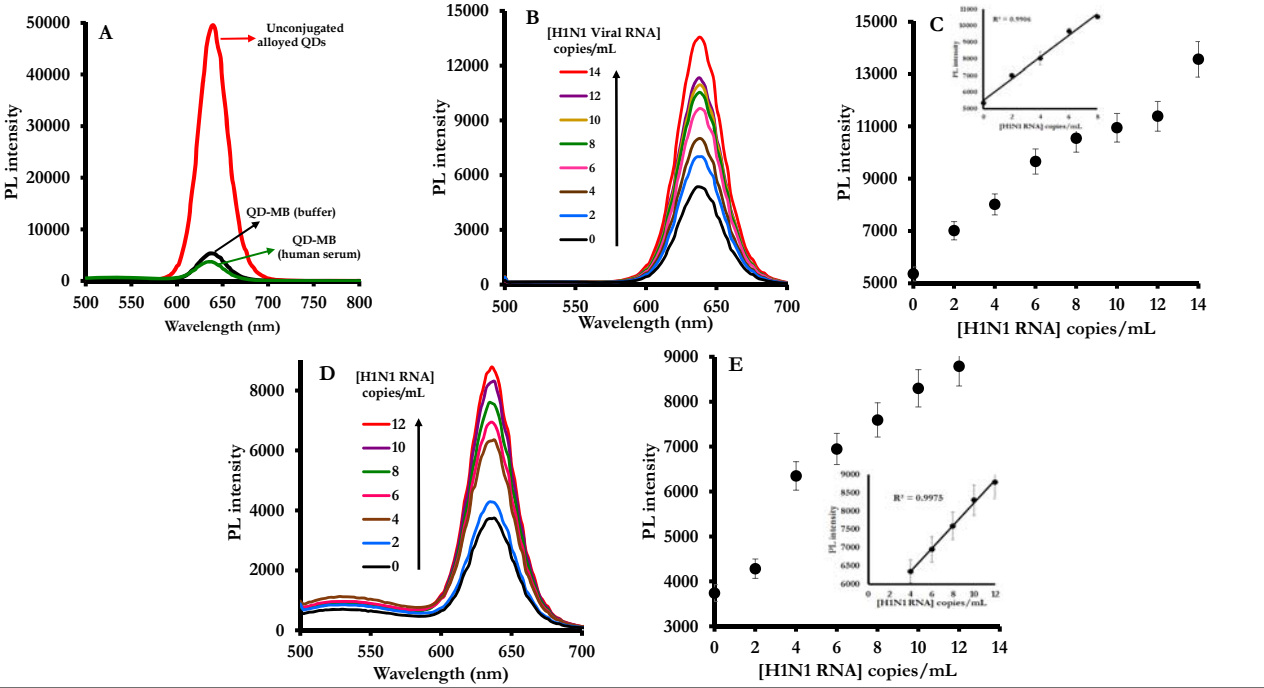

Fig. 8, Adegoke et al.

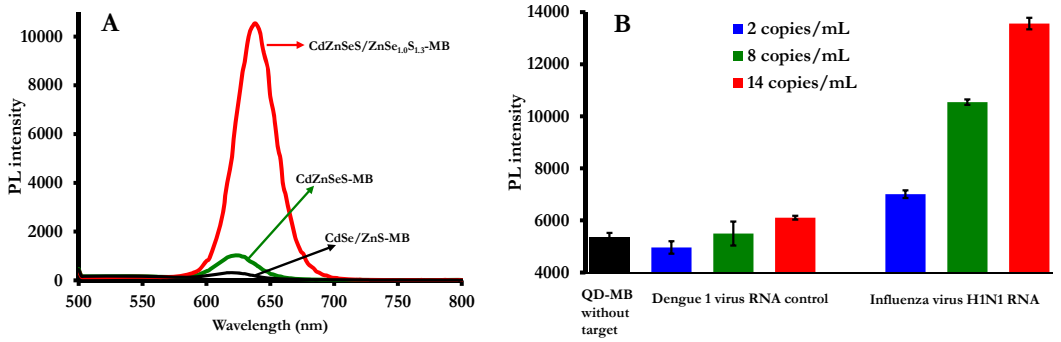

SUPPLEMENTARY INFORMATION

Gradient band gap engineered alloyed quaternary/ternary CdZnSeS/ZnSeS quantum dots: An ultrasensitive fluorescence reporter in a conjugated molecular beacon system for the biosensing of influenza virus RNA

Oluwasesan Adegoke,[1] Min-woong Seo,[2] Tatsuya Kato,[3] Shoji Kawahito,[2] Enoch Y. Park[1,3,1]

[1] Laboratory of Biotechnology, Research Institute of Green Science and Technology, Shizuoka University, 836 Ohya, Suruga-ku, Shizuoka 422-8529, Japan

[2] Imaging Devices Laboratory, Research Institute of Electronics, Shizuoka University, Johoku 3-5-1,Naka-ku, Hamamatsu 432-8011, Japan

[3] Laboratory of Biotechnology, Department of Applied Biological Chemistry, Faculty of Agriculture, Shizuoka University, 836 Ohya, Suruga-ku, Shizuoka 422-8529, Japan

E-mail:
adegoke.sesan@mailbox.co.za (O. Adegoke)
kato.tatsuya@shizuoka.ac.jp (T. Kato)
park.enoch@shizuoka.ac.jp (E.Y. Park)

[1] Correspondence: Laboratory of Biotechnology, Department of Applied Biological Chemistry, Faculty of Agriculture, Shizuoka University, 836 Ohya, Suruga-ku, Shizuoka 422-8529, Japan. E-mail: park.enoch@shizuoka.ac.jp

A

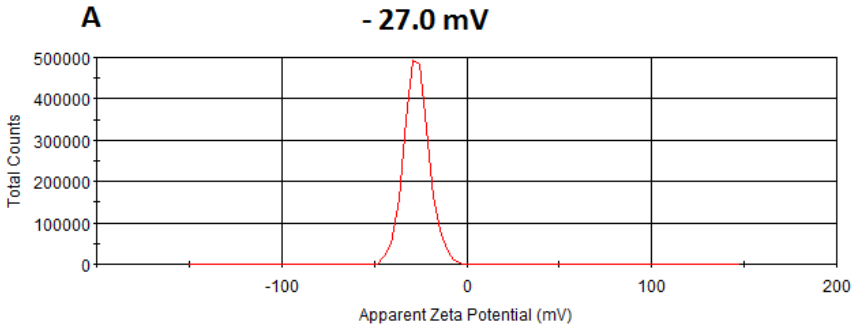
- 27.0 mV
500000
400000
300000
200000
100000
0
Total Counts
-100
0
100
200
Apparent Zeta Potential (mV)

B

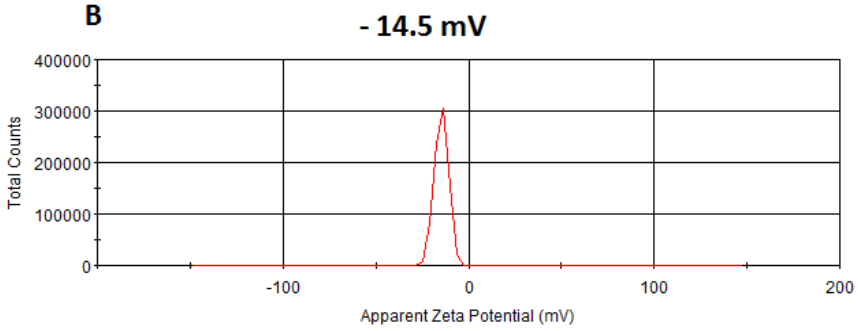
- 14.5 mV
400000
300000
200000
100000
0
Total Counts
-100
0
100
200
Apparent Zeta Potential (mV)

C

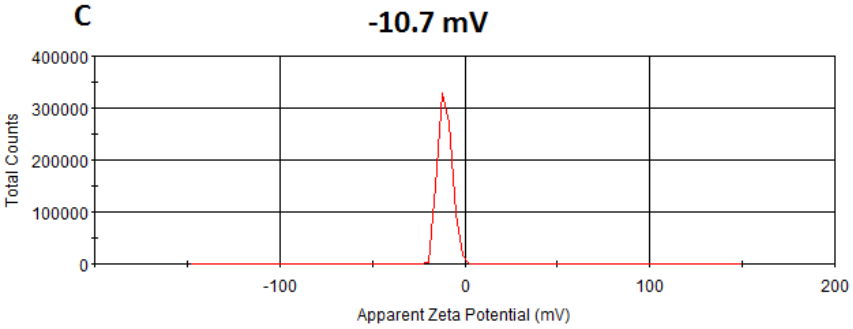
-10.7 mV
400000
300000
200000
100000
0
Total Counts
-100
0
100
200
Apparent Zeta Potential (mV)

D

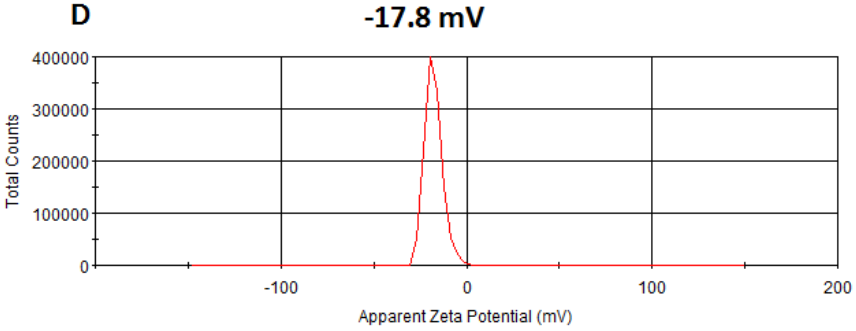
-17.8 mV
400000
300000
200000
100000
0
Total Counts
-100
0
100
200
Apparent Zeta Potential (mV)

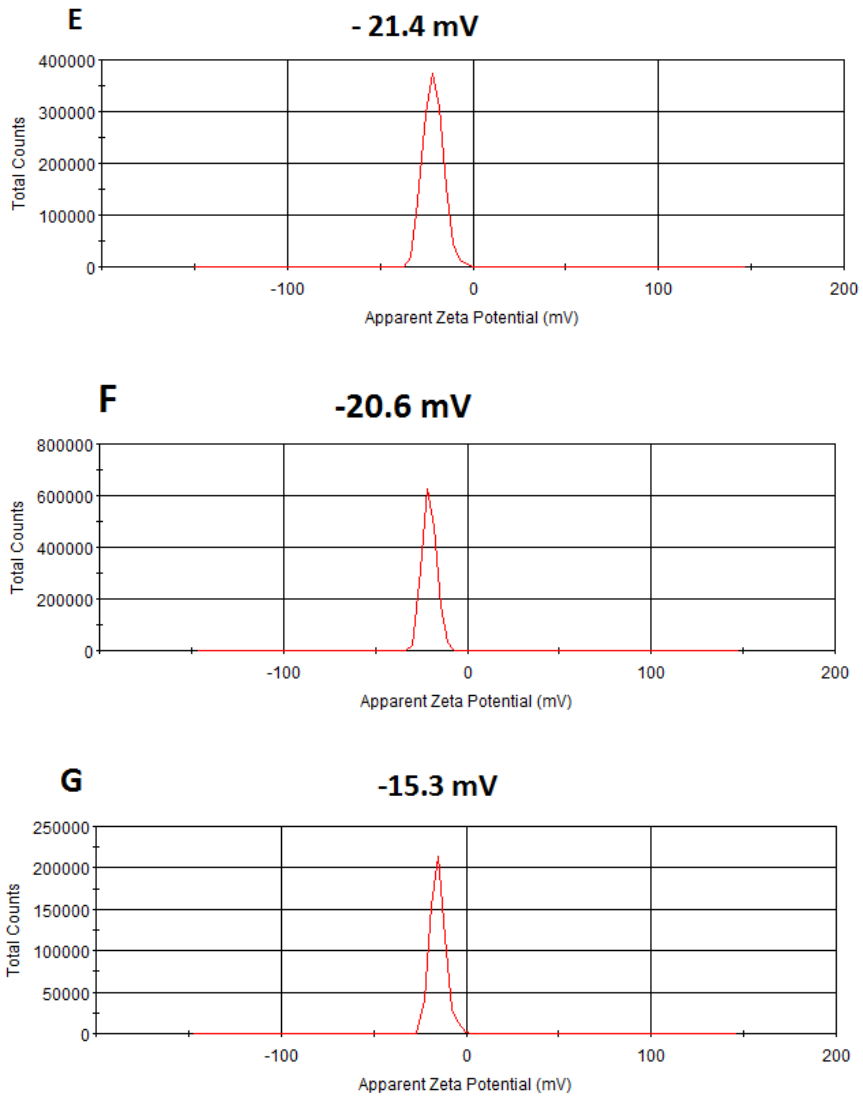

Fig. S-1. Zeta potential curves for alloy TGA-capped (A) CdZnSeS, (B) $CdZnSeS/ZnSe_{1.0}S_{1.3}$, (C) $CdZnSeS/ZnSe_{1.0}S_{1.4}$, (D) $CdZnSeS/ZnSe_{1.0}S_{1.5}$, (E) $CdZnSeS/ZnSe_{1.0}S_{1.6}$, (F) $CdZnSeS/ZnSe_{1.0}S_{1.7}$ and (G) $CdZnSeS/ZnSe_{1.0}S_{1.8}$ QDs.

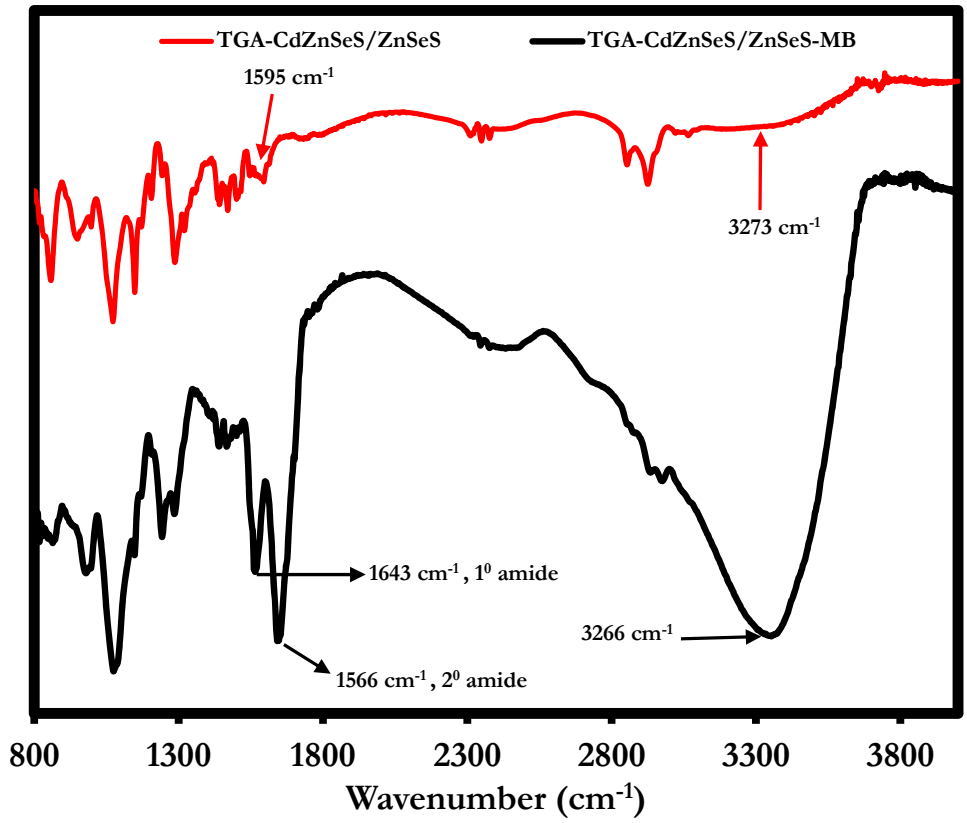

Fig. S-2. FT-IR spectra of the unconjugated QDs and the QD-MB bioprobe.